ISSN 1674-1056
http://cpb.iphy.ac.cn
http://iopscience.iop.org/cpb
中国物理 B
Chinese Physics B

Rydberg quantum controlled-phase gate with one control and multiple target qubits

S L Su(苏石磊)

Citation: Chin. Phys. B . 2018, 27(11): 110304. **doi:** 10.1088/1674-1056/27/110304

Journal homepage: http://cpb.iphy.ac.cn; http://iopscience.iop.org/cpb

What follows is a list of articles you may be interested in

Two-qubit pure state tomography by five product orthonormal bases

Yu Wang(王宇), Yun Shang(尚云)
Chin. Phys. B . 2018, 27(10): 100306. **doi:** 10.1088/1674-1056/27/10/100306

Deterministic hierarchical joint remote state preparation with six-particle partially entangled state

Na Chen(陈娜), Bin Yan(颜斌), Geng Chen(陈赓), Man-Jun Zhang(张曼君), Chang-Xing Pei(裴昌幸)
Chin. Phys. B . 2018, 27(9): 090304. **doi:** 10.1088/1674-1056/27/9/090304

Phase precision of Mach-Zehnder interferometer in PM2.5 air pollution

Duan Xie(谢端), Haifeng Chen(陈海峰)
Chin. Phys. B . 2018, 27(7): 070304. **doi:** 10.1088/1674-1056/27/7/070304

Classical-driving-assisted coherence dynamics and its conservation

De-Ying Gao(高德营), Qiang Gao(高强), Yun-Jie Xia(夏云杰)
Chin. Phys. B . 2018, 27(6): 060304. **doi:** 10.1088/1674-1056/27/6/060304

Fractal dynamics in the ionization of helium Rydberg atoms

Xiulan Xu(徐秀兰), Yanhui Zhang(张延惠), Xiangji Cai(蔡祥吉), Guopeng Zhao(赵国鹏), Lisha Kang(康丽莎)
Chin. Phys. B . 2016, 25(11): 110301. **doi:** 10.1088/1674-1056/25/11/110301

Rydberg quantum controlled-phase gate with one control and multiple target qubits*

S L Su(苏石磊)†

School of Physics and Engineering, Zhengzhou University, Zhengzhou 450001, *China*

(Received 29 June 2018; revised manuscript received 22 August 2018; published online 19 October 2018)

We propose a scheme to construct the multiple-qubit Rydberg quantum controlled-phase gate with one control and multiple target qubits. The proposed quantum logic gate works under the asymmetric-Rydberg-interaction-induced dipole blockade and can be implemented with three operation steps. The most prominent characteristic of the scheme is that the required operation time and steps keep invariant as the number of qubits increases. The Rydberg state leakage and some practical situations are considered. The Lindblad master equation is used to evaluate and verify the feasibility of the scheme.

Keywords: Rydberg atom, quantum logic gate, Rydberg–Rydberg interaction

PACS: 03.67.–a, 03.67.Lx, 32.80.Ee **DOI:** 10.1088/1674-1056/27/11/110304

1. Introduction

Due to the advances in experimental operation, especially trapping and cooling, Rydberg atoms have received much attention in the research of quantum information. When they are excited to Rydberg states with high principal quantum number[1,2] and close enough, strong Rydberg–Rydberg interaction (RRI) arises. Consequently and interestingly, a frequency matched classical laser field cannot excite more than one atom,[3,4] which is called Rybderg blockade and has been observed in experiments with two Rydberg atoms located about 4 μm[5] apart by collective driving and 10 μm[6] apart through sequent driving, respectively. The RRI has also been directly measured in experiment.[7] Via contactless RRI, the photonic nonlinear dynamics is obtained in experiment.[8] Besides, two-qubit Rydberg logic gates can be constructed via the RRI induced energy shift,[9] phase shift,[10] blockade phenomenon,[11–18] Rydberg dressing,[19–23] generalized Rabi frequency,[24] or two-atom dark state method.[25] Recently, new Rydberg regimes[26–29] and quantum controls of the pulses[30,31] have also been designed for the Rydberg quantum gate.

Multiple-qubit quantum logic gates are meaningful for quantum algorithm and quantum information processing.[32–34] The conventional gate-decomposition protocols imply that a multiple-qubit quantum logic gate can be decomposed into single- and two-qubit gates.[34–36] However, the number of required single- and two-qubit quantum gates increases dramatically as the number of qubits in multiple-qubit logic gates increases. Constructing the multiple-qubit quantum logic gate directly is worth studying[37–43] because more quantum resources would be saved. The conventional n-qubit controlled-phase performs a phase operation on a target qubit depending on the state of the rest $n-1$ control qubit, which has wide applications in complex quantum algorithms[44] and quantum error correction.[45,46] Besides, the n-qubit controlled-phase with one control and $n-1$ target qubits also has extensive applications in quantum entangled state preparation,[47] quantum error correction,[48] the discrete cosine transform,[49] and quantum cloning,[50] and has been constructed through multiple-step[51–53] or single-step[54] via a virtual photon process. In addition to the atom–cavity system, the cross-Kerr nonlinearity system is also a promising platform for quantum information processing[55–58] and can be used to construct the one control and multiple target qubits quantum logic gate[59,60] on the premise that the perfect singe-photon resource is achieved.[61–64] Based on Rydberg blockade, several schemes have been proposed for the construction of conventional multiple-qubit Rydberg quantum logic gates via exciting atoms into different Rydberg states,[65] considering asymmetric Rydberg interactions,[66,67] and sequent driving based Rydberg collective excitation.[68] In contrast, a multiple-qubit quantum logic gate with one control qubit and multiple target qubits has not been well-studied in the Rydberg atom system.

Inspired by these studies, we propose a scheme to construct the multiple-qubit Rydberg quantum controlled-phase gate with one control and multiple-target qubits. The asymmetric-RRI-based blockade regime[69,70] and the well-defined laser coupling sequences[3,4] make the required conditional dynamics realizable. The required operation step and the operation time are kept invariant as the qubit number increases.

*Project supported by the National Natural Science Foundation of China (Grant No. 11747096).

†Corresponding author. E-mail: slsu@zzu.edu.cn

© 2018 Chinese Physical Society and IOP Publishing Ltd

2. Controlled-phase gate with one control and multiple target qubits

2.1. Three-qubit case

Figure 1(a) illustrates the schematic diagram of the n-qubit controlled-phase gate. For clearness, we first consider the case; i.e., two target Rydberg atoms $(2,3)$ interacting with the control Rydberg atom 1. The Hamiltonians of atoms 1 and k $(k=2,3)$ are (set $\hbar=1$)

$$\hat{H}_1=\frac{\Omega_1}{2}\mathrm{e}^{\mathrm{i}\phi}|1\rangle_1\langle R|+\mathrm{H.c.},\quad \hat{H}_k=\frac{\Omega_k}{2}|1\rangle_k\langle r|+\mathrm{H.c.} \tag{1}$$

Besides, the RRI Hamiltonian is

$$\hat{H}_V=\sum_{k=2}^{3}V_{Rr}(\hat{\sigma}_1^{Rr}\otimes\hat{\sigma}_k^{rR}+\mathrm{H.c.})+V_{rr}\hat{\sigma}_2^{rr}\otimes\hat{\sigma}_3^{rr}, \tag{2}$$

in which $\hat{\sigma}_j^{ab}$ denotes $|a\rangle\langle b|$ of the j-th atom. The first term of Eq. (2) denotes the resonant dipole–dipole interactions while the second term denotes the van der Waals (vdW) interactions.[16,69] The dipole–dipole-interaction-induced blockade[4] is critical for the scheme, the whole scheme requires three steps.

Step (i) Apply a π pulse on Rydberg atom 1 and set $\phi=0$. The first term of Hamiltonian (1) works and the transition $|1\rangle_1\rightarrow-\mathrm{i}|R\rangle_1$ is achieved.

Step (ii) Apply 2π pulses on the rest of the Rydberg atoms 2 and 3. The last term of Hamiltonian (1) works. Suppose the conditions $V_{Rr}\gg\Omega_{1(k)}\gg V_{rr}$[69] are satisfied, then the transitions $|\alpha\beta\rangle_{23}\rightarrow(-1)^{\alpha}(-1)^{\beta}|\alpha\beta\rangle_{23}$ are achieved if the initial state of atom 1 is $|0\rangle_1$, where $\alpha,\beta\in\{0,1\}$. The blockade effect induced by V_{rr} is ignored due to the condition $\Omega_k\gg V_{rr}$. Otherwise, if the initial state of atom 1 is $|1\rangle_1$, then it would be excited to $|R\rangle$ after step (i). The role of $|r\rangle_k$-mediated 2π pulse is inhibited due to the blockade effect induced by V_{Rr}. Then, the transitions $|\alpha\beta\rangle_{23}\rightarrow|\alpha\beta\rangle_{23}$ are achieved.

Step (iii) Apply a π pulse on Rydberg atom 1 and set $\phi=\pi$. The first term of Hamiltonian (1) works and the transition $|R\rangle_1\rightarrow\mathrm{i}|1\rangle_1$ is achieved. Thus, the whole evolution process can be illustrated as

$$\begin{aligned}&|0\alpha\beta\rangle_{123}\rightarrow(-1)^{\alpha}(-1)^{\beta}|0\alpha\beta\rangle_{123},\\&|1\alpha\beta\rangle_{123}\rightarrow|1\alpha\beta\rangle_{123},\end{aligned} \tag{3}$$

which is the desired three-qubit logic gate. Although a quantum logic gate with one control and multiple target qubits has unique applications in quantum information, it is also interesting to find the relation between the studied quantum logic gate and the universal quantum logic gate. In Fig. 2, we take the three-qubit case as an example to reveal the relations between the universal Toffoli gate (left side) and the constructed logic gate (in the dot-dashed frame on the right side).

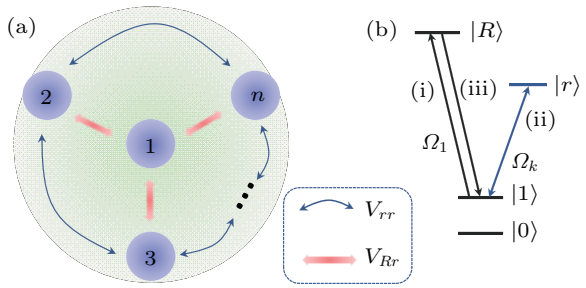


Fig. 1. (color online) (a) Schematic diagram of the controlled-phase gate with one control and multiple target qubits. (b) Energy level and the corresponding laser coupling for control (1) and target ($k=2,3,\ldots,n$) atoms. $\Omega_{1(k)}$ is the Rabi frequency of the transitions $|1\rangle\leftrightarrow|R(r)\rangle$ of atom $1(k)$. $|R\rangle$ denotes high-lying Rydberg state. The principal quantum number of the Rydberg state $|r\rangle$ is not equal to that of $|R\rangle$, which induces the asymmetric RRI strength $V_{Rr}\gg V_{rr}$ (suppose $V_{Rr}(V_{rr})$ is identical for different target atoms for simplicity) through choosing different energy levels, as described in Ref. [69]. $|0\rangle$ and $|1\rangle$ are two ground states used to encode the quantum information.

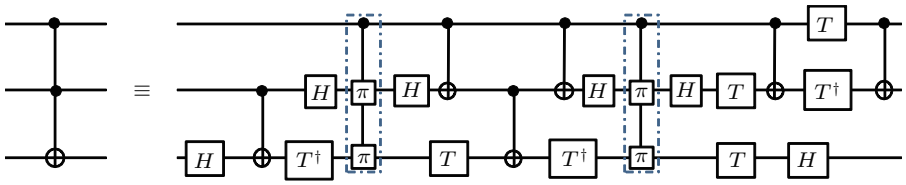


Fig. 2. The relation between the constructed quantum logic gate (on the right-hand side, dot-dashed frame) and the universal quantum Toffoli gate (on the left-hand side). $T=\mathrm{e}^{\mathrm{i}\pi\hat{\sigma}_z/8}$. H denotes Hardmard gate.

2.2. The n-qubit case

The scheme is easy to be extended to the n-qubit case ($k=2,3,\ldots,n$). The Hamiltonians (1) keep invariant while the RRI Hamiltonian should be changed to ($k>k'$)

$$\hat{H}_V=\sum_{k=2}^{n}V_{Rr}(\hat{\sigma}_1^{Rr}\otimes\hat{\sigma}_k^{rR}+\mathrm{H.c.})+\sum_{k,k'}^{n}V_{rr}|rr\rangle_{kk'}\langle rr|. \tag{4}$$

After considering the asymmetric RRI, the interactions among the target atoms do not affect the evolutions induced by the classical field since $\Omega_k\gg V_{rr}$. Nevertheless, the state of Rydberg atom 1 influences the evolution of all of the target atoms since the condition $V_{Rr}\gg\Omega_k$ is satisfied and the blockade effect emerges if both of the control and target atoms are initially in state $|1\rangle$. After the same three steps, the n-qubit quantum gate with one control qubit and $n-1$ target qubits

$$\begin{aligned}&|0\alpha\beta\cdots\varsigma\rangle_{123\cdots n}\rightarrow(-1)^{\alpha}(-1)^{\beta}\cdots(-1)^{\varsigma}|0\alpha\beta\cdots\varsigma\rangle_{123\cdots n},\\&|1\alpha\beta\cdots\varsigma\rangle_{123\cdots n}\rightarrow|1\alpha\beta\cdots\varsigma\rangle_{123\cdots n}\end{aligned} \tag{5}$$

is achieved.

3. Discussion

One of the features of the scheme is that the total required operation time is not increased with increasing qubit number. Two factors influence the performance of the scheme. One is the blockade error, the other is the dissipation originated from spontaneous emission. The blockade error should be considered from two aspects. First, V_{Rr} should be strong enough to blockade the target Rydberg atoms to be excited to $|r\rangle$ if the control and some or all of the target atoms are initially in state $|1\rangle$. Second, the RRI strength V_{rr} should be weak enough to allow collective excitation of the target atoms if the control atom is initially in state $|0\rangle$ and some or all of the target atoms are initially in state $|1\rangle$. Generally speaking, the evolution of the whole system can be described by the Markovian master equation

$$\dot{\hat{\rho}} = -\mathrm{i}[\hat{H},\hat{\rho}] + \frac{\gamma}{2}\sum_{m=1}^{n}\sum_{l=0}^{1}\left[2\hat{\sigma}_{ml}\hat{\rho}\hat{\sigma}_{ml}^{\dagger} - \hat{\rho}\hat{\sigma}_{ml}^{\dagger}\hat{\sigma}_{ml} - \hat{\sigma}_{ml}^{\dagger}\hat{\sigma}_{ml}\hat{\rho}\right], \quad (6)$$

where $\hat{\sigma}_{ml} = |l\rangle_m\langle R(r)|$ denotes the decay process from state $|R(r)\rangle$ to ground states of atom m, and γ is the atomic spontaneous emission rate. If we calculate the fidelity through Eq. (6) with Hamiltonian (1) involved V_{1k} and $V_{kk'}$, and dissipation terms involved γ, then the influence of the above two factors on the final gate fidelity will arise naturally.

3.1. Asymmetric Rydberg interactions

Rydberg asymmetric interactions have been used and studied for efficiently achieving multi-particle entanglement by Saffman and Mølmer[69] via blockade regime based on unitary dynamics, Carr and Saffman[70] via antiblockade regime based on dissipation, and for construction of three-qubit Toffoli gate by Brion *et al.*[65] Since dipole–dipole interaction strength V_{Rr} is approximate to $n^4/\mathcal{R}^3$ and vdW interaction strength V_{rr} is approximate to $n^{11}/\mathcal{R}^6$, where n and $\mathcal{R}$ denote principal quantum number and distance between Rydberg atoms, respectively, the strongly asymmetric Rydberg interactions can be readily met by choosing sufficiently large $\mathcal{R}$ and sufficiently small n, whose lower limit is scaled by the blackbody limited spontaneous emission lifetime $\tau \sim n^2$.[69] More specifically, One can obtain the calculated blockade strength from Fig. 3 extracted from Ref. [69], which shows that the asymmetry Rydberg interctions can be achieved well because V_{Rr} is at least 150 times bigger than V_{rr}. Specifically, one can find that V_{Rr} would be 1000 times bigger than V_{rr} if the angle of the molecular axis is around 30°.[69] That is, it is reasonable if we choose $V_{Rr} = [100, 400] \times V_{rr}$ in the following analysis and numerical calculations.

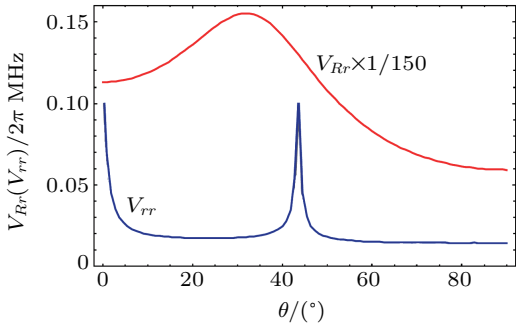


Fig. 3. (color online) Calculated blockade strength in Ref. [69] as a function of the angle θ of the molecular axis for ^{87}Rb atom. For the exact values of atomic characteristic length, magnetic field and energy levels, see Fig. 2 in Ref. [69].

3.2. Average fidelity

To estimate the performance of the quantum controlled-phase gates more accurately, the average fidelity rather than the fidelity obtained from one group of specific initial state and the corresponding final state should be used. We use two methods to measure the average fidelity. The first one is given by Nielsen[71] and White *et al.*[72] with the form

$$\overline{F}(\varepsilon,\hat{U}) = \frac{\sum_j \mathrm{tr}(\hat{U}\hat{U}_j^{\dagger}\hat{U}^{\dagger}\varepsilon(\hat{U}_j)) + d^2}{d^2(d+1)}, \quad (7)$$

where $\hat{U}_j$ is the tensor of Pauli matrices $\underbrace{\hat{I}\hat{I}\cdots\hat{I}}_{n},\underbrace{\hat{I}\cdots\hat{X}}_{n},\ldots,\underbrace{\hat{Z}\cdots\hat{Z}}_{n}$ for n-qubit quantum logic gate, $\hat{U}$ is the perfect phase gate, $d = 2^n$, and ε is the trace-preserving quantum operation obtained by our logic gate whose value can be obtained through numerically solving Eq. (6). The second is to calculate the mean value of the fidelities corresponding to several groups of random initial states*

$$\overline{F} = \frac{1}{k}\sum_{m=1}^{k}\left[\mathrm{Tr}\sqrt{\sqrt{\hat{\rho}_m^{\mathrm{ideal}}}\hat{\rho}_m(t)\sqrt{\hat{\rho}_m^{\mathrm{ideal}}}}\right]^2, \quad (8)$$

where $\rho_m(t)$ denotes the practical output density matrix correspond to the random m-th input state, and ρ_m^{ideal} is the corresponding matrix obtained from the ideal controlled-phase gate. In Fig. 4, we plot the average fidelity of the three-qubit quantum logic gate obtained via the two different methods, which shows that the scheme has high fidelities. In Fig. 5, we plot four- and five-qubit quantum logic gates, respectively, with the density matrix obtained from one group of specific initial states to save the time of numerical simulation. The results show that although the performance decreases as the number of the qubits increases, the fidelity is always higher than 97% with perfect blockade condition $w = q = 20$.

*We use *rand* command in matlab to produce the random initial state.

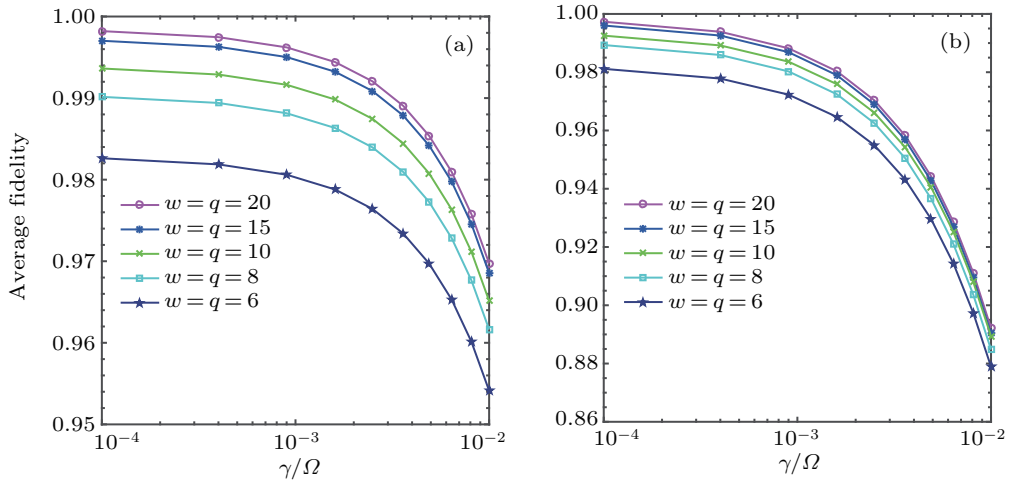


Fig. 4. (color online) Average fidelities of the three-qubit quantum controlled-phase gate versus atomic spontaneous rate γ based on (a) trace-operator and (b) random initial states methods with one hundred of random initial states. For simplicity, we set $\Omega_1 = \Omega_2 = \Omega_3 = \Omega$, $V_{Rr} = w\Omega$, $\Omega = qV_{rr}$, and $w = q$ without loss of generality.

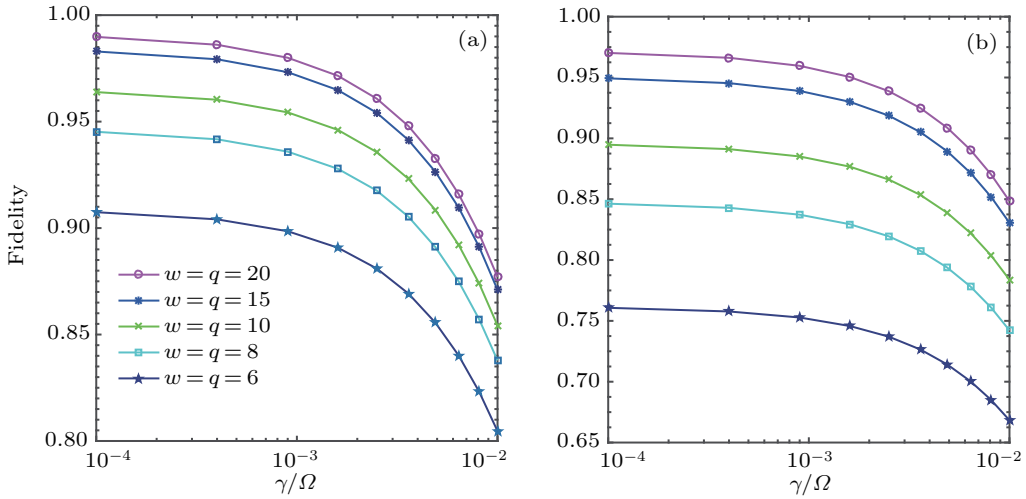


Fig. 5. (color online) Fidelities of the (a) four- and (b) five-qubit quantum controlled-phase gates versus atomic spontaneous rate γ based on the final density matrix $\hat{\rho}^{\text{ideal}}$ obtained by the ideal quantum logic gate and practically final density matrix $\hat{\rho}$ obtained through the system dynamics governed by Eq. (6) with the specific initial states $\sum_{i=1}^{4(5)} \otimes(|0\rangle+|1\rangle)_i/\sqrt{2}$, in which $F = \left[\text{Tr}\sqrt{\sqrt{\hat{\rho}^{\text{ideal}}}\hat{\rho}\sqrt{\hat{\rho}^{\text{ideal}}}}\right]^2$ is used. For simplicity, we set $\Omega_1 = \Omega_2 = \Omega_3 = \Omega_4 = \Omega_5 = \Omega$, $V_{Rr} = w\Omega$, $\Omega = qV_{rr}$, and $w = q$ without loss of generality.

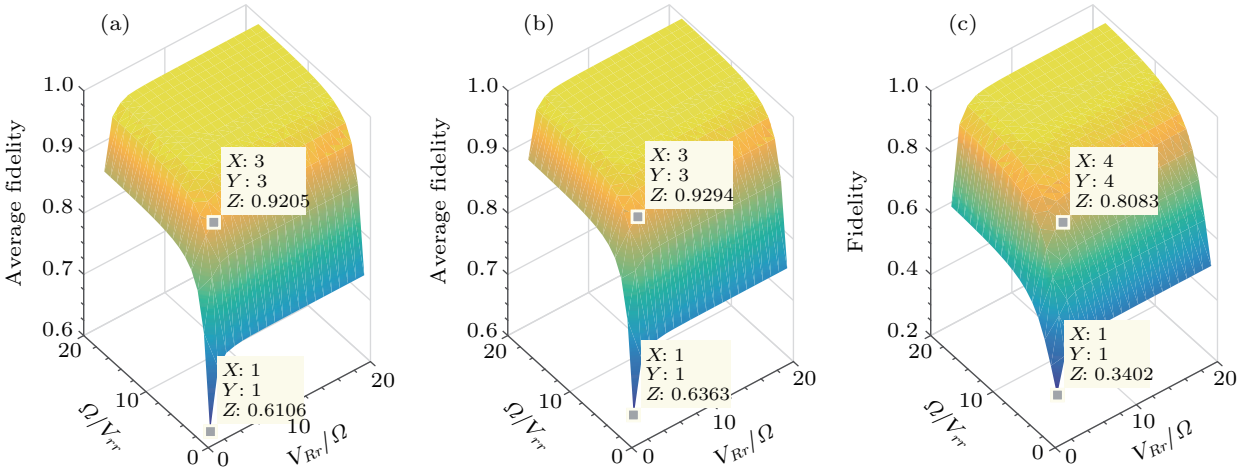


Fig. 6. (color online) Average fidelities of the three-qubit quantum controlled-phase gate based on (a) random initial states method and (b) trace-operator method with one hundred of random initial states versus V_{Rr}/Ω and Ω/V_{rr}. For simplicity, we set $\Omega_1 = \Omega_2 = \Omega_3 = \Omega_4 = \Omega$. (c) Fidelity of the four-qubit quantum controlled-phase gate with the initial state being set as $\sum_{i=1}^{4} \otimes[(|0\rangle+|1\rangle)_i/\sqrt{2}]$. The dissipative rate $\gamma/\Omega = 10^{-3}$ is used.

3.3. Influence of an imperfect blockade

As discussed earlier, V_{Rr} should be strong enough to block the target atoms once the control atom is excited and V_{rr} should be weak enough to allow collective excitations of the target atoms if the control atom is not excited. We now use the numerical methods to estimate the influence of the imperfect blockade. In Fig. 6, we take the three- and four-qubit cases as examples to study this influence. One can find that the three-qubit case has good robustness under imperfect RRI strength. The fidelity of the four-qubit case can still be higher than 0.8 with $w = q = 4$ although the robustness of the four-qubit case is not better than that of the three-qubit case.

3.4. Robustness of the parameters' variation

In the previous discussion, we suppose that the parameters keep invariant. Practically, the parameters would no doubt fluctuate during the experiment. Without loss of generality, we assume that the fluctuation of the parameter satisfies a Gaussian distribution with mean value p and standard deviation δp. For a fixed δp, we consider 100 groups of p_j that satisfy the Gaussian distribution. For a given p_j, we get the corresponding fidelity F_j at the optimal time through Eq. (7) for the trace-operator-based method and through Eq. (8) for the random-initial-state-based method. Then, the mean value is calculated as $\bar{F} = \sum_{j=1}^{j=100} F_j/100$. In addition, the standard deviation of F_j is calculated based on the 100 sets of data for the given δp. In Fig. 7, we plot the variations of the average fidelity versus $\delta V_{Rr}/V_{Rr}$ and $\delta V_{rr}/V_{rr}$, respectively. The results show the good robustness of the scheme on the fluctuations of the RRIs.

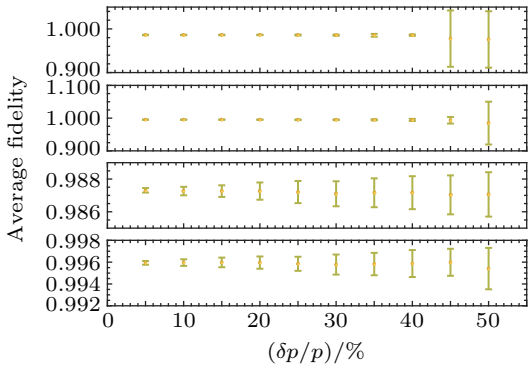


Fig. 7. (color online) The variations of the average fidelities versus scaled standard deviations of inhomogeneous parameter p. (a) $p = V_{Rr}$, random-initial-based-method. (b) $p = V_{Rr}$, trace-operator-based method. (c) $p = V_{rr}$, random-initial-based-method. (d) $p = V_{rr}$, trace-operator-based method. The standard parameters are chosen as $V_{Rr}/\Omega = 18$, $\Omega/V_{rr} = 20$, and $\gamma = 10^{-3}\Omega$. For the random-initial-based method, 100 groups of normalized initial states are considered.

3.5. Atomic transition errors

Practically, atomic transition error arises when the near-resonant coupling to other unwanted states happens. To estimate the average fidelities under this situation, we consider two near-resonant transition channels following the spirit of Ref. [25], in which all possible dipole allowed transitions with the change of principal quantum number up to ± 5 from the resonant states are considered.

We consider the leakage channels as shown in Fig. 8. The possible choices of the Rydberg atom pair states and the corresponding experimentally feasible parameters are extracted from Ref. [25]. In Table 1, for the four-qubit case, we use non-Hermitian Hamiltonian and Schrödinger equation rather than Lindblad master equation for simulation to save the computation space. And V_{rr} is supposed to be $0.02V_{Rr}$. The results show that under the influence of the Rydberg state leakage, the fidelity can still be higher than 0.99. One should note that, in the practical case, the condition $V_{Rr} \gg V_{rr}$ should be reconsidered with the data in Table 1. The vdW is induced by the non-resonant dipole–dipole interaction with the form[74]

$$\hat{H}_{\rm vdW} = \sum_s \frac{|rr\rangle\langle rr|\hat{H}^s_{\rm dd}|rs\rangle\langle rs|\hat{H}^s_{\rm dd}|rr\rangle\langle rr|}{\delta_s} = V_{rr}|rr\rangle\langle rr|, \quad (9)$$

in which $\hat{H}^s_{\rm dd}$ denotes the non-resonant dipole–dipole interaction Hamiltonian with detuning δ_s related to Rydberg state $|s\rangle$, $\hat{H}_{\rm vdW}$ denotes the vdW Hamiltonian, and $|s\rangle$ denotes the possible Rydberg state that may be coupled to $|r\rangle$ via the dipole–dipole interaction. From Eq. (9), one can obtain that the accurate way to achieve the vdW interaction is to sum up all of the possible Rydberg states $|s\rangle$ that couple to $|R\rangle$ with the non-resonant dipole–dipole interaction. If the detuning δ_s of one group of specific dipole–dipole interaction is small, then the condition $V_{rr} \ll V_{Rr}$ may not be satisfied. Nevertheless, from the point that the electric field can induce resonant dipole–dipole interaction, one can also set an electric field to enlarge δ_s and further weaken V_{rr}.

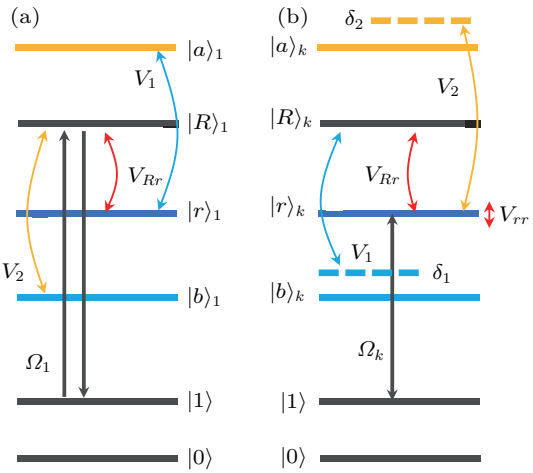


Fig. 8. (color online) Energy levels, laser couplings, and the RRIs of (a) the control atom and (b) the target atoms used to construct the n-qubit controlled-phase gate. $|R\rangle$, $|r\rangle$ $|a\rangle$, and $|b\rangle$ denote the Rydberg states. $|R\rangle_1|r\rangle_k \to |b\rangle_1|a\rangle_k$ with defect δ_2 and strength V_2, and $|r\rangle_1|R\rangle_k \to |a\rangle_1|b\rangle_k$ with defect δ_1 and strength V_1. V_{Rr} is the strength of the dipole–dipole interaction between the control and target atoms. V_{rr} is the strength of the vdW interaction among the target atoms. The scheme requires $V_{Rr} \gg V_{rr}$,[69] which can be achieved by using Förster resonances and choosing suitable $\mathcal{R}$ and n.[73] The Rydberg state $|a\rangle$- and $|b\rangle$-induced transitions, as well as the vdW interactions V_{rr} give rise to the transition errors. $\Omega_{1(k)}$ is the Rabi frequency of the transitions $|1\rangle \leftrightarrow |R\rangle_1$ ($|1\rangle \leftrightarrow |r\rangle_k$) of control atom 1 (target atom k). $|0\rangle$ and $|1\rangle$ constitute the computation subspace.

Table 1. Average fidelity $\overline{F}$ of the n-qubit quantum logic gate versus n and RRI strength with the consideration of atomic transition leakage errors and dissipation. $|r\rangle_1|R\rangle_k \to |a\rangle_1|b\rangle_k$ and $|R\rangle_1|r\rangle_k \to |b\rangle_1|a\rangle_k$ are two leakage channels. To make states $|R\rangle_1|r\rangle_k$ and $|r\rangle_1|R\rangle_k$ degenerate, the external static electric fields E (V/m) should be 14.2, 5.36, and 20.1 (from top to bottom), respectively. The states are specified as nl_jm with n, l, and m being the principal, angular, and magnetic quantum numbers, respectively. The corresponding DD coefficients C_3 (GHz·μm^3) are calculated as −68.2, 65.3, and −51.4, respectively, and V_{Rr}/γ equals 38.5, 35.5, and 23.1, respectively, at the temperature of 4 K. The interatomic separation is assumed to be 3 μm between the control and target atoms. The fourth-order variable step-size Runge–Kutta algorithm is used to solve the master equation.

Resonant	$\|a\rangle_1$	$\|b\rangle_k$	V_1/V_{Rr}	δ_1/MHz	$\|b\rangle_1$	$\|a\rangle_k$	V_2/V_{Rr}	δ_2/MHz	n	$\overline{F}_{\text{leakage}}$
$\|R\rangle_1 \equiv 112s_{1/2}1/2$ $\|r\rangle_k \equiv 101s_{1/2}1/2$ $\|r\rangle_1 \equiv 112p_{3/2}3/2$ $\|R\rangle_k \equiv 101p_{3/2}3/2$	$111d_{5/2}5/2$	$99d_{5/2}5/2$	−0.64	−471.239	$112p_{1/2}(-1/2)$	$101p_{3/2}(-1/2)$	−0.49	1074.425	2 3 4	0.9906992 0.9781971 0.9407130
$\|R\rangle_1 \equiv 111p_{3/2}3/2$ $\|r\rangle_k \equiv 101p_{3/2}3/2$ $\|r\rangle_1 \equiv 112s_{1/2}1/2$ $\|R\rangle_k \equiv 101s_{1/2}1/2$	$111p_{1/2}(-1/2)$	$101p_{1/2}(-1/2)$	0.66	−1627.345	$110d_{5/2}5/2$	$100d_{5/2}5/2$	−2.17	12503.539	2 3 4	0.9986263 0.9780258 0.9396703
$\|R\rangle_1 \equiv 105p_{3/2}3/2$ $\|r\rangle_k \equiv 94p_{3/2}3/2$ $\|r\rangle_1 \equiv 105s_{1/2}1/2$ $\|R\rangle_k \equiv 94s_{1/2}1/2$	$105p_{1/2}(-1/2)$	$94p_{3/2}(-1/2)$	−0.49	1551.947	$104d_{5/2}5/2$	$92d_{5/2}5/2$	−0.64	−1162.389	2 3 4	0.9983958 0.9760406 0.9400395

3.6. Other possible schemes to construct the controlled-phase gate

The scheme may be improved through introducing other methods, such as electromagnetically induced transparency (EIT) and geometric controls. In this subsection, we will describe some of the possible schemes and provide corresponding parameter ranges, which maybe useful for further studies.

3.6.1. EIT-based scheme

The performance of the scheme may be improved based on the EIT[11,75] method. To do this, as shown in Fig. 9(a), a metastable state $|p\rangle$ is introduced to couple with $|r\rangle$ and $|1\rangle$ with Rabi frequencies Ω_E and Ω_k, respectively. This scheme requires the condition $V_{Rr} \gg \Omega_E \gg \Omega_{1(k)} \gg V_{rr}$ to be satisfied. The transfer process $|1\rangle \to |p\rangle \to |1\rangle$ is inhibited if $\Omega_E \gg \Omega_k$ (known as EIT) when the control atom is initially in state $|0\rangle$. On the other hand, if the control atom is excited to $|R\rangle$, the EIT would be destroyed. The whole process can be divided into the following four cases (We here take two-qubit as an example to illustrate the dynamical process). (I) For the initial state $|0\rangle|0\rangle$, it stays invariant because it is decoupled with the laser. (II) For the initial state $|0\rangle|1\rangle$, it would be invariant because the control atom is decoupled to the laser coupling, and the transition of the target atom $|1\rangle \to |p\rangle$ is transparent to the laser due to the EIT condition $\Omega_E \gg \Omega_{(k)}$. (III) For the initial state $|1\rangle|0\rangle$, the control atom would be transformed to the Rydberg state after step (i) and further be transformed to $|1\rangle$ after step (iii). The state of the target atom is decoupled and stays invariant. (IV) For the initial state $|1\rangle|1\rangle$, the control atom would be transformed to the Rydberg state after step (i). The EIT regime of the target atom would be destroyed due to the strong RRI condition $V_{Rr} \gg \Omega_E$. Then after step (ii), the target atom would obtain a π phase. After step (iii), the state would be changed to $-|1\rangle|1\rangle$. We note that the scheme can be directly generalized to multiple-qubit case if the condition $\Omega_{1(k)} \gg V_{rr}$ is satisfied since the interactions between the multiple target atoms can be discarded and they can thus be considered independently. That is, the quantum logic operation would be achieved after the three steps.

3.6.2. Geometric phases

The other robust method is to use the geometric operations.[76] As shown in Fig. 9(b), we can choose $\Omega_k = -\Omega \sin(\theta/2)\, e^{i\phi}$ and $\Omega_E = \Omega \cos(\theta/2)$. If the control parameters θ and ϕ vary smoothly to satisfy the adiabatic condition and θ equals 0 at the starting and ending points, then state $|1\rangle$ would obtain a geometric phase $\varphi = (\oint \sin\theta \, d\theta \, d\phi)/2$ after the cyclic evolution.[77] It should be noted that the vdW blockade would influence the geometric controls since the condition $\{\Omega_k, \Omega_E\} \gg V_{rr}$ is not always satisfied at the starting and ending points.

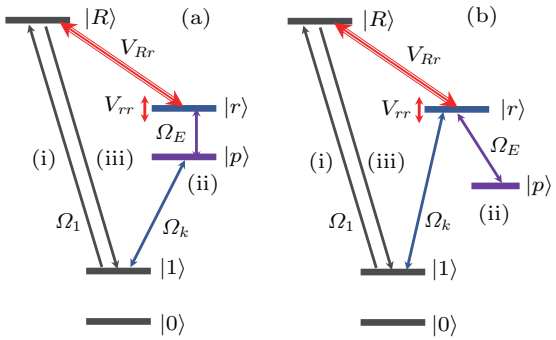


Fig. 9. (color online) (a) The EIT-based scheme. (b) Geometric phase scheme.

4. Conclusion

Based on the asymmetric-RRI-induced blockade regime, we proposed a scheme to construct the multiple-qubit controlled-phase gate with one control and multiple-target qubits. Analysis with the master equation method showed that the scheme is robust to RRI fluctuation. In addition, the required operation step and time of the scheme are not increased with the increase of the qubit number in the quantum logic gate. We have also shown that the proposed scheme can be generalized to the EIT and the geometric phase cases. We

hope that the proposed multiple-qubit controlled-phase gate can find some applications in the future Rydberg-atom-based QIP tasks with the development of technology.

Acknowledgment

S. L. Su would like to thank Dr. H. Z. Shen for our useful discussions.

References

[1] Gallagher T F 1994 *Rydberg Atoms* (Cambridge: Cambridge University Press)
[2] Saffman M, Walker T G and Mølmer K 2010 *Rev. Mod. Phys.* **82** 2313
[3] Jaksch D, Cirac J I, Zoller P, Rolston S L, Côté R and Lukin M D 2000 *Phys. Rev. Lett.* **85** 2208
[4] Lukin M D, Fleischhauer M, Côté R, Duan L M, Jaksch D, Cirac J I and Zoller P 2001 *Phys. Rev. Lett.* **87** 037901
[5] Gaëtan A, Miroshnychenko Y, Wilk T, Chotia A, Viteau M, Comparat D, Pillet P, Browaeys A and Grangier P 2009 *Nat. Phys.* **5** 115
[6] Urban E, Johnson T A, Henage T, Isenhower L, Yavuz D D, Walker T G and Saffman M 2009 *Nat. Phys.* **5** 110
[7] Béguin L, Vernier A, Chicireanu R, Lahaye T and Browaeys A 2013 *Phys. Rev. Lett.* **110** 263201
[8] Busche H, Huillery P, Ball S W, Ilieva T, Jones M P A and Adams C S 2017 *Nat. Phys.* **13** 655
[9] Brion E, Pedersen L H and Mølmer K 2007 *J. Phys. B: At. Mol. Opt. Phys.* **40** S159
[10] Shi X F and Kennedy T A B 2017 *Phys. Rev. A* **95** 043429
[11] Müller M, Lesanovsky I, Weimer H, Büchler H P and Zoller P 2009 *Phys. Rev. Lett.* **102** 170502
[12] Isenhower L, Urban E, Zhang X L, Gill A T, Henage T, Johnson T A, Walker T G and Saffman M 2010 *Phys. Rev. Lett.* **104** 010503
[13] Kuznetsova E, Bragdon T, Côté R and Yelin S F 2012 *Phys. Rev. A* **85** 012328
[14] Xia T, Zhang X L and Saffman M 2013 *Phys. Rev. A* **88** 062337
[15] Goerz M H, Halperin E J, Aytac J M, Koch C P and Whaley K B 2014 *Phys. Rev. A* **90** 032329
[16] Bhaktavatsala Rao D D and Mølmer K 2014 *Phys. Rev. A* **89** 030301(R)
[17] Maller K M, Lichtman M T, Xia T, Sun Y, Piotrowicz M J, Carr A W, Isenhower L and Saffman M 2015 *Phys. Rev. A* **92** 022336
[18] Das S, Grankin A, Iakoupov A, Brion E, Borregaard J, Boddeda R, Usmani I, Ourjoumtsev A, Grangier P and Sørensen A S 2016 *Phys. Rev. A* **93** 040303(R)
[19] Keating T, Cook R L, Hankin A M, Jau Y Y, Biedermann G W and Deutsch I H 2015 *Phys. Rev. A* **91** 012337
[20] Müller M M, Murphy M, Montangero S, Calarco T, Grangier P and Browaeys A 2014 *Phys. Rev. A* **89** 032334
[21] Petrosyan D and Mølmer K 2014 *Phys. Rev. Lett.* **113** 123003
[22] Keating T, Goyal K, Jau Y Y, Biedermann G W, Landahl A J and Deutsch I H 2013 *Phys. Rev. A* **87** 052314
[23] Shao X Q, Li D X, Ji Y Q, Wu J H and Yi X X 2017 *Phys. Rev. A* **96** 012328
[24] Shi X F 2017 *Phys. Rev. Applid.* **7** 064017
[25] Petrosyan D, Motzoi F, Saffman M and Mølmer K 2017 *Phys. Rev. A* **96** 042306
[26] Su S L, Liang E J, Zhang S, Wen J J, Sun L L, Jin Z and Zhu A D 2016 *Phys. Rev. A* **93** 012306
[27] Su S L, Tian Y, Shen H Z, Zang H, Liang E and Zhang S 2017 *Phys. Rev. A* **96** 042335
[28] Su S L, Shen H Z, Liang E J and Zhang S 2018 *Phys. Rev. A* **98** 032306
[29] Li D X and Shao X Q arXiv:1806.05336
[30] Huang X R, Ding Z X, Hu C S, Shen L T, Li W, Wu H and Zheng S B arXiv:1806.09775v1
[31] Kang Y H, Chen Y H, Shi Z C, Huang B H, Song J and Xia Y 2018 *Phys. Rev. A* **97** 042336
[32] Toffoli T 1980 *Lectures Notes in Computer Science* (de Bakker J W and van Leeuwen J, Ed.) Vol. 84 (New York: Springer)
[33] Fredkin E and Toffoli T 1982 *Int. J. Theor. Phys.* **21** 219-253
[34] Nielsen M A and Chuang I L 2000 *Quantum Computation and Quantum Information* (Cambridge: Cambridge University Press)
[35] Barenco A, Bennett C H, Cleve R, DiVincenzo D P, Margolus N, Shor P, Sleator T, Smolin J A and Weinfurter H 1995 *Phys. Rev. A* **52** 3457
[36] Saeedi M and Pedram M 2013 *Phys. Rev. A* **87** 062318
[37] Chen C Y, Feng M and Gao K L 2006 *Phys. Rev. A* **73** 064304
[38] Zhang Y Q and Zhang S 2009 *Chin. Phys. B* **18** 4683
[39] Tang S Q, Zhang D Y, Xie L J, Zhan X G and Gao F 2009 *Chin. Phys. B* **18** 56
[40] Xiao Y F, Zou X B and Guo G C 2007 Phys. Rev. A **75** 014302
[41] Shao X Q, Zhu A D, Zhang S, Chung J S and Yeon K H 2007 *Phys. Rev. A* **75** 034307
[42] Monz T, Kim K, Hänsel W, Riebe M, Villar A S, Schindler P, Chwalla M, Hennrich M and Blatt R 2009 *Phys. Rev. Lett.* **102** 040501
[43] Zheng S B 2013 *Phys. Rev. A* **87** 042318
[44] Vandersypen L M K, Steffen M, Breyta G, Yannoni C S, Sherwood M H and Chuang I L 2001 *Nature* **414** 883
[45] Cory D G, Price M D, Maas W, Knill E, Laflamme R, Zurek W H, Havel T F and Somaroo S S 1998 *Phys. Rev. Lett.* **81** 2152
[46] Sarovar M and Milburn G J 2005 *Proc. SPIE Int. Soc. Opt. Eng.* **5842** 158
[47] Šašura M and Bužek V 2001 *Phys. Rev. A* **64** 012305
[48] Gaitan F 2008 *Quantum Error Correction and Fault Tolerant Quantum Computing* (New York: CRC Press)
[49] Beth T and Rotteler M 2001 *Quantum Information* Vol. 173, Chapter 4, page 96 (Berlin: Springer)
[50] Braunstein S L, Bužek V and Hillery M 2001 *Phys. Rev. A* **63** 052313
[51] Yang C P, Liu Y X and Nori F 2010 *Phys. Rev. A* **81** 062323
[52] Yang C P, Zheng S B and Nori F 2010 *Phys. Rev. A* **82** 062326
[53] Yang C P, Su Q P and Liu J M 2012 *Phys. Rev. A* **86** 024301
[54] Yang C P, Su Q P, Zhang F Y and Zheng S B 2014 *Opt. Lett.* **39** 3312
[55] Nemoto K and Munro W J 2004 *Phys. Rev. Lett.* **93** 250502
[56] Lin Q and Li J 2009 *Phys. Rev. A* **79** 022301
[57] Shen C P, Gu X F, Guo Q, Zhu, X Y, Su S L and Liang E J 2018 *J. Opt. Soc. A. B* **35** 694
[58] Su S L, Wang Y, Guo Q, Wang H F and Zhang S 2012 *Chin. Phys. B* **21** 044205
[59] Xiu X M, Li Q Y, Lin Y F, Dong L, Dong H K and Gao Y J 2017 *Opt. Commun.* **393** 173
[60] Dong L, Lin Y F, Cui C, Dong H K, Xiu X M and Gao Y J 2018 *Quantum Inf. Process.* **17** 114
[61] Shen H Z, Zhou Y H and Yi X X 2014 *Phys. Rev. A* **90** 023849
[62] Shen H Z, Zhou Y H and Yi X X 2015 *Phys. Rev. A* **91** 063808
[63] Shen H Z, Li D X, Su S L, Zhou Y H and Yi X X 2017 *Phys. Rev. A* **96** 033805
[64] Shen H Z, Shang C, Zhou Y HandYi X X 2018 *Phys. Rev. A* **98** 023856
[65] Brion E, Mouritzen A S and Mølmer K 2007 *Phys. Rev. A* **76** 022334
[66] Wu H Z, Yang Z B and Zheng S B 2010 *Phys. Rev. A* **82** 034307
[67] Isenhower L, Saffman M and Mølmer K 2011 *Quantum Inf. Process.* **10** 755
[68] Su S L, Gao Y, Liang E and Zhang S 2017 *Phys. Rev. A* **95** 022319
[69] Saffman M and Mølmer K 2009 *Phys. Rev. Lett.* **102** 240502
[70] Carr A W and Saffman M 2013 *Phys. Rev. Lett.* **111** 033607
[71] Nielsen M A 2002 *Phys. Lett. A* **303** 249
[72] White A G, Gilchrist A, Pryde G J, O'Brien J L, Bremner M J and Langford N K 2007 *J. Opt. Soc. Am. B* **24** 172
[73] Beterov I I and Saffman M 2015 *Phys. Rev. A* **92** 042710
[74] Walker T G and Saffman M 2008 *Phys. Rev. A* **77** 032723
[75] Weimer H, Müller M, Lesanovsky I, Zoller P and Büchler H P 2010 *Nat. Phys.* **6** 382
[76] Wu H Z, Huang X R, Hu C S, Yang Z B and Zheng S B 2017 *Phys. Rev. A* **96** 022321
[77] Duan L M, Cirac J I and Zoller P 2001 *Science* **292** 1695